DC AND AC MICROGRIDS FOR MINING APPLICATIONS

Paper No. PCIC-

Galina Mirzaeva
Senior Member, IEEE
The University of Newcastle
Callaghan NSW2308
Australia
galina.mirzaeva@newcastle.edu.au

Dmitry Miller
PhD, Engineer
Ampcontrol CSM
Cameron Park NSW2285
Australia
dmitry.miller@ampcontrolgroup.com

Abstract – The commitment of mining industry to reduction of greenhouse gas emissions necessitates enhancements in operational efficiency, electrification, and renewable-energy use. An effective way to integrate renewable resources into a mining electrical system is to utilize microgrids. This paper reviews DC and AC microgrid technologies, with a focus on coordination mechanisms between distributed generators, to achieve equitable sharing of the load power demand.

The paper then discusses a specific (current-driven) control strategy for DC or AC microgrids, which uses minimal (or no) communication. The paper shows that, under this strategy, distributed generators of different ratings act in a coordinated manner and exhibit identical, first-order dynamics. Furthermore, the microgrid control is stable in the presence of any load types.

The paper further discusses integration of Power Line Communication into the current-driven load sharing control. This can be used to redistribute inequalities in distributed generation resulting from faults and changed conditions. The technologies discussed in the paper offer distinct benefits to mining and other industries. Findings of the paper are supported by simulations.

Index Terms — Microgrids, Decentralized control, Power converter control, Distributed power generation, Mining industry.

I. INTRODUCTION[1]

The impact of mining on climate change has been a topic of discussion over the past decade [1]. A significant share of greenhouse-gas (GHG) emissions is associated with combustion of fossil fuels. This share of global emissions can be reduced, in long-term, via altering the demand for mining commodities [2]. Another area of concern, fugitive methane emissions from coal mining, can be tackled by advancing the methane capture and utilization technologies [3].

This paper focuses on the third source of GHG emissions, which is related to the mining operations and power consumption. Full decarbonization in this area can be achieved through operational efficiency, electrification, and renewable-energy use. A large proportion of mining machines are already fully electrical. This includes surface mining equipment (e.g., rope shovels, draglines) as well as underground mining machines (e.g., continuous miners, coal loaders, haulers, etc.). A large scope exists for using more electricity and alternative (e.g., hydrogen) forms of energy in mining trucks [4].

Moving to renewable sources in electricity generation in mining is becoming increasingly feasible. A number of large mining companies across the world demonstrate effective use of solar energy. A key technology in both renewable energy integration and transport electrification is microgrid. A microgrid can be briefly described as “a group of interconnected loads and distributed energy resources, that acts as a single controllable entity” [5]. One major difference between a solar farm and a microgrid with solar energy is that microgrids generally aim to supply local loads without grid connection.

As long as the locally generated power (by the microgrid sources, or distributed generators (DG)) is enough to supply the local loads, the microgrid would stay disconnected from the grid, or in “islanded mode”. If the locally generated power is not sufficient, then the “deficit” can be obtained from the grid. If the locally generated power exceeds the local needs, then the “excess” can be exported to the grid. From the grid perspective, the microgrid is either invisible, appears like a load or appears like a generator, respectively. Incorporation of energy storage into the microgrid helps using the “excess” power during “deficit” periods, which further reduces the need for the microgrid to stay grid connected.

Providing the described functionality requires an appropriate design of the microgrid control. Due to the similarities between microgrids and traditional power systems, the starting point in microgrid control has been to mimic concepts that have been successful in the traditional grid, such as power-frequency droop control and a hierarchical structure consisting of primary, secondary, and tertiary levels [6]. This structure, applied to microgrid control, is shown in Fig.1. The control levels have the following functions.

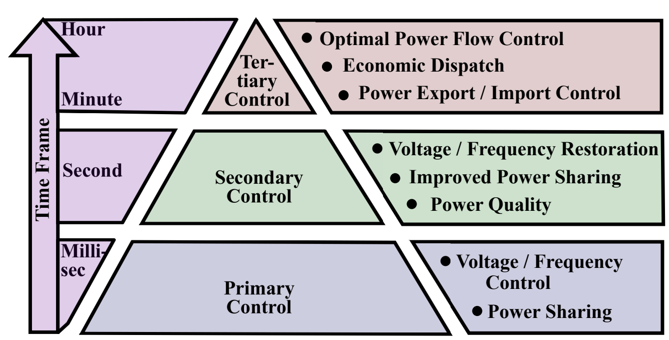

Fig. 1 Microgrid control hierarchy

[1] This research was partially supported by the Australian Government through the Australian Research Council's Discovery Projects funding scheme (project DP190103307).

1) The main function of *Primary Control* is to share active and reactive power consumed by the loads, between the distributed generators (DGs). To avoid dependence on high bandwidth communications, this is commonly based on the droop control principle [7], with active (P) and reactive (Q) powers being functions of the microgrid frequency (f) and bus voltage magnitude (V), respectively. Each DG can infer the microgrid loading condition with knowledge of the system V and f values, and adjust its P and Q output accordingly.

2) *Secondary Control* corrects frequency/voltage set points (f^*, V^*) affected by droop control. It can also regulate the power sharing targets for each DG. This helps, for example, when some DGs come into or out of operation. Another important function is power quality action. This refers to the compensation of harmonics and phase unbalance introduced by non-linear and unbalanced loads. Secondary Control is achieved by using low-bandwidth communications [8].

3) *Tertiary Control* is used for power import/export from/to the grid in grid-connected mode. Scheduling of these power exchanges according to economic goals may involve Optimal Power Flow and/or Economic Dispatch tasks. Tertiary Control uses low-bandwidth communications.

While the hierarchical structure described above has its merits, it introduces unnecessary complexity when controlling small and medium size microgrids. Hence, a recent trend in the microgrid control literature is to utilize a reduced structure with only two levels [9], [10], [11]. Power sharing and power quality control are achieved at the bottom level, and power exchange between microgrid and utility is handled by the top level. Examples of such control include mining or mining relevant applications, such as on-board microgrids for electric transport [12], standalone emergency microgrids [13], power conditioning [14], and general microgrids that incorporate renewable sources and reduce carbon emissions [15], [16].

Both AC and DC microgrids are of interest for mining applications: AC - due to their compatibility with the existing infrastructure, and DC - due to their superior efficiency and stability [17]. An AC microgrid in "islanded" (disconnected from the grid) mode is illustrated in Fig.2, where three control options (excluding Tertiary Control) are presented.

Fig.2(a) illustrates the droop control concept where each Distributed Generators (DG) is connected to the common microgrid AC bus via a voltage-controlled converter (VCC). Each VCC is provided with the voltage and current measurements. Variation of the common microgrid V and f is the necessary part of the droop mechanism. Restoration of V and f to their nominal values, and other supervisory functions, are achieved by Secondary Control via low bandwidth communication.

The Master-Slave control principle is shown in Fig.2(b). The Master DG is connected to the microgrid bus via a VCC. It regulates the microgrid V and f around their constant and nominal values. In doing so, it determines the required current demand and then distributes it between itself and Slaves - DGs connected via current controlled converters (CCC).

The currents references (i^*_{Sj}), that are sent from Master to Slaves, may include fundamental component, as well as harmonic and unbalance compensation. Thus the need for the Secondary Control level is completely eliminated. The resulting control structure is simple, stable and robust. On the other hand, to provide real-time power sharing, communication from Master to Slaves must be very fast (or high bandwidth).

The third control architecture, a current-driven power sharing shown in Fig.2(c), is the primary focus of this paper. It combines the advantages of the previous two principles and avoids their main disadvantages. Specifically, a VCC-connected DG, typically associated with battery storage, provides constant V and f of the microgrid bus. No communication links exist between the VCC and the current controlled DGs.

There is no droop control, hence V and f restoration to nominal values is unnecessary. Shares in the fundamental, harmonic and unbalance currents are inferred by each current controlled DG from the real-time measurement of their respective downstream currents. Furthermore, the microgrid has a simple first-order system behaviour, which remains stable in the presence of any loads. This includes active loads connected via power converters called in the literature Constant Power Loads (CPL) [18], that are well-known for their destabilizing effect on droop controlled microgrids.

The above advantages are achieved by smart utilization of a radial microgrid architecture, as discussed in the next section.

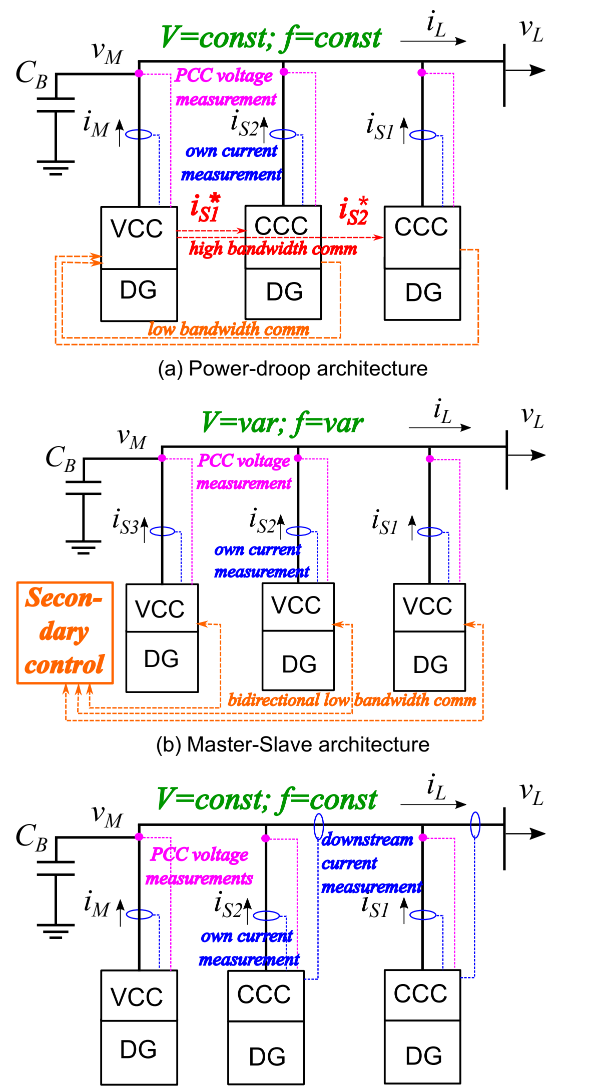

(a) Power-droop architecture

(b) Master-Slave architecture

(c) Current-driven power sharing architecture

Fig. 2 Comparison of three microgrid architectures

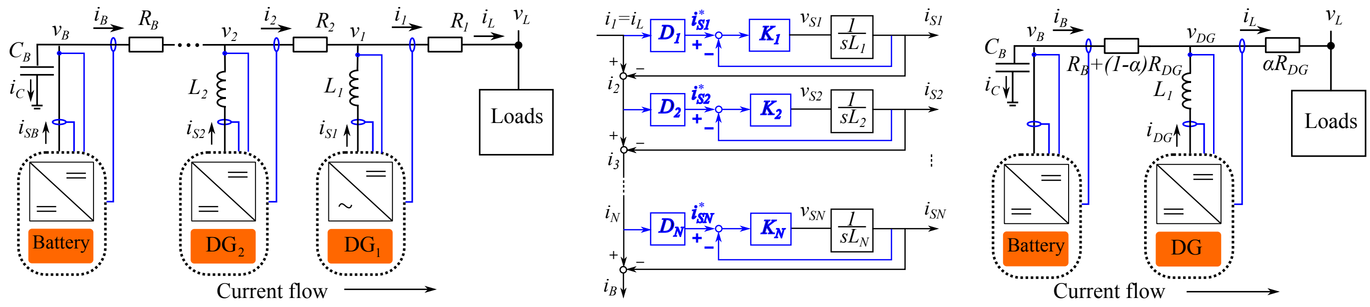

(a) DC microgrid connection and measurement (b) DC microgrid control diagram (c) DC microgrid equivalent scheme

Fig. 3 DC microgrid under current-driven power sharing

II. PRINCIPLES OF CURRENT-DRIVEN POWER SHARING

In this section, principles of the current-driven power sharing are explained using a DC microgrid model, as shown in Fig.3(a). The DC option is a preferred model for standalone, local microgrids not reliant on the existing AC infrastructure.

Distributed sources DG1, DG2, ... shown in Fig.3(a) can be of any nature (AC or DC). They are connected to the common microgrid DC bus via current controlled converters (DC/DC or AC/DC) and coupling inductances L_1, L_2, ... The leftmost, voltage-controlled DG is associated with capacitive and/or battery storage. It is assumed to only supply transient currents.

The first aim of the current-driven power sharing is to provide an automatic sharing of the load current by the current controlled DG1, DG2, ..., in proportion to their ratings. The share of each DG can be defined with respect to the total load current (i_L) or with respect to its downstream current (i_1, i_2, ...) measured to the right from the coupling point. Thus defined shares, E_j and D_j, respectively, can be found for each DG as:

$$E_j = \frac{S_j}{\sum_{k=1}^{N} S_k} \qquad\qquad D_j = \frac{S_j}{\sum_{k=j}^{N} S_k} \tag{1}$$

where S_j is the power rating of the DGj.

For example, if four identical current controlled DGs carry equal shares in the total load current then $E_j = 1/4\ (j = 1, \dots, 4)$. The rightmost DG1 supplies $D_1 = 1/4$ of its downstream current; the next DG2 supplies $D_2 = 1/3$; DG3 supplies $D_3 = 1/2$; and DG4 (the leftmost DG just before the battery) supplies $D_4 = 1$ of the downstream current that it measures.

The measured downstream current for each DGj is then multiplied by share D_j defined in (1) and the result is supplied to the DG current control as its desired current reference i_{Sj}^*. This is illustrated in Fig.3(b). In the coloured version of the paper, different colours are used to distinguish between physical flows and devices (such as currents, inductances, etc.) and measured/calculated quantities and numeric blocks (such as current references, shares and gains). Current control for DGj loops around gain K_j and coupling inductance L_j, represented by its transfer function $(1/sL_j)$.

The second aim of the power sharing scheme is to achieve an identical dynamic response by all DGs in a multi-inverter system, irrespective of their nature, size and power ratings. An exponential response with a common time constant τ would lead to a simple and stable first-order dynamics.

Say that load current $i_L = i_1$ undergoes a step change from i_L^o to i_L^s values. As the step change commences, the reference current for DG1 (the closest to the load) becomes equal to $D_1 i_L^s$. Then the voltage across the coupling inductor L_1 is:

$$L_1 \frac{di_{S1}}{dt} = K_1(D_1 i_L^s - i_{S1}) \tag{2}$$

For DG2, the reference current obtained from the current stream, becomes equal to $D_2 i_2 = D_2(i_L^s - i_{S1})$. The voltage across its coupling inductor L_2 equals:

$$L_2 \frac{di_{S2}}{dt} = K_2(D_2 i_L^s - D_2 i_{S1} - i_{S2}) \tag{3}$$

Repeating the same derivation for all current controlled DGs leads to a triangular system (6). Solution to the first equation of system (6), or (2), can be obtained independently as (note that $D_1 = E_1$):

$$i_{S1}(t) = D_1\left[i_L^o e^{-t\frac{K_1}{L_1}} + i_L^s\left(1 - e^{-t\frac{K_1}{L_1}}\right)\right] \tag{4}$$

The control gain K_1 is chosen so that time constant $\tau = L_1/K_1$. Next, substituting (4) into (3) and finding its solution by using the method of undetermined coefficients, yields

$$i_{S2}(t) = D_2 i_L^s(1 - D_1) + \frac{\frac{K_2}{L_2} D_2 D_1 (i_L^o - i_L^s)}{\frac{K_1}{L_1} - \frac{K_2}{L_2}} e^{-t\frac{K_1}{L_1}} + Ce^{-t\frac{K_2}{L_2}} \tag{5}$$

Note two exponential dynamics, $e^{-t\frac{K_1}{L_1}}$ and $e^{-t\frac{K_2}{L_2}}$, present in (5). By selecting an appropriate value of gain K_2, the second dynamic should be suppressed, and the first dynamic should be further manipulated into a form similar to (4). By substituting the

$$\frac{d}{dt}\begin{bmatrix} i_{S1} \\ i_{S2} \\ \vdots \\ i_{S(N-1)} \end{bmatrix} = \begin{bmatrix} -\frac{K_1}{L_1} & 0 & \cdots & 0 \\ -\frac{K_2}{L_2} D_2 & -\frac{K_2}{L_2} & \cdots & 0 \\ \vdots & \vdots & \ddots & 0 \\ -\frac{K_{N-1}}{L_{N-1}} D_{N-1} & -\frac{K_{N-1}}{L_{N-1}} & \cdots & -\frac{K_{N-1}}{L_{N-1}} \end{bmatrix} \begin{bmatrix} i_{S1} \\ i_{S2} \\ \vdots \\ i_{S(N-1)} \end{bmatrix} + \begin{bmatrix} \frac{K_1}{L_1} D_1 \\ \frac{K_2}{L_2} D_2 \\ \vdots \\ \frac{K_{N-1}}{L_{N-1}} D_{N-1} \end{bmatrix} \tag{6}$$

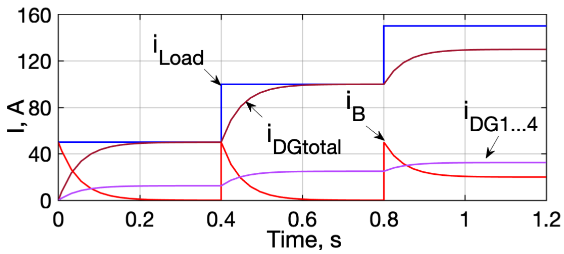

(a) Equal DG inverter currents

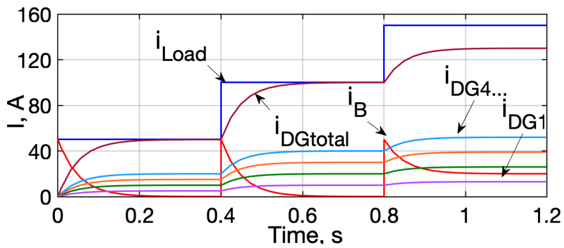

(b) Unequal DG inverter currents

Fig. 4 Response to load step changes of the example microgrid

initial condition $i_{S2}(0) = D_2 i_L^o (1 - D_1)$ into (5), and setting $K_2 = K_1(1 - D_1)\, L_2/L_1$, results in the following DG2 response:

$$i_{S2}(t) = D_2(1 - D_1)\left[i_L^o e^{-t\frac{K_1}{L_1}} + i_L^s\left(1 - e^{-t\frac{K_1}{L_1}}\right)\right] \quad (7)$$

Note similarity between (7) and (4), as well as the fact that $(1 - D_1) = E_2/D_2$. Repeating the same procedure for the next DG, etc., it can be shown that the following condition must be met to ensure the same dynamics of each DGj:

$$K_j = \frac{L_j}{L_1} K_1 \sum_{k=j}^{N} S_k / \sum_{k=1}^{N} S_k = \frac{L_j}{L_1} K_1 \frac{E_j}{D_j} \quad (8)$$

If condition (8) is satisfied, then current supplied by DGj can be described as:

$$i_{Sj}(t) = E_j\left[i_L^o e^{-\frac{t}{\tau}} + i_L^s\left(1 - e^{-\frac{t}{\tau}}\right)\right] \quad (9)$$

where $\tau = L_1/K_1$.

The combined current supplied by all current controlled DGs is given by:

$$i_{DG}(t) = \sum_{j=1}^{N} i_{Sj} = i_L^o e^{-\frac{t}{\tau}} + i_L^s\left(1 - e^{-\frac{t}{\tau}}\right) \quad (10)$$

The transient current supplied by the leftmost voltage-controlled DG (battery) is given by

$$i_B(t) = i_L(t) - i_{DG}(t) = (i_L^s - i_L^o) e^{-\frac{t}{\tau}} \quad (11)$$

In frequency domain, expressions (9)-(11) correspond to:

$$i_{Sj} = E_j \frac{1}{1+s\tau} i_L \qquad i_{DG} = \frac{1}{1+s\tau} i_L \qquad i_B = \frac{s\tau}{1+s\tau} i_L \quad (12)$$

As follows from expressions (9)-(10), all current controlled DGs have identical dynamics; and the combination of N differently rated current-controlled DG inverters behaves like a single first-order system. Then the microgrid connected as shown in Fig.3(a) can be represented by a simplified microgrid with one equivalent DG and one battery, as shown in Fig.3(c). The load side voltage can then be obtained as:

$$v_L(t) = v_{PCC} - (R_B + R_{DG}) i_B(t) - \alpha R_{DG} i_{DG}(t) \quad (13)$$

where v_{PCC} is voltage at the point of common coupling, controlled at constant and nominal level;

R_B is resistance of the battery section of the DC bus as shown in Fig.3(a);

$R_{DG} = R_1 + R_2 + \ldots + R_N$ is the total resistance of the DG section of the DC bus; and αR_{DG} is its equivalent resistance (since not all DG currents flow through the total resistance R_{DG}, then $\alpha < 1$).

It can be noted that synchronism between the current controlled DGs is achieved without any communication, just by using the downstream current measurement for reference generation and by setting their control gains according to (8).

Following the previous example, assume that four current controlled DGs have equal ratings and coupling inductances. Then, in order for them to share the load current equally, their gains need to be set as: K_1; $K_2 = 0.75K_1$; $K_3 = 0.5K_1$; $K_4 = 0.25K_1$. Their response to step changes of the load current is illustrated by simulation in Fig.4(a).

Another example includes four differently sized DGs with equal inductances. They are expected to share the load current as 0.1; 0.2; 0.3; 0.4. According to (8), the corresponding current control gains should be set as: K_1; $K_2 = 0.9K_1$; $K_3 = 0.7K_1$; $K_4 = 0.4K_1$. Fig.4(b) shows the corresponding dynamic simulation.

In both examples in Fig.4, the total capacity of all four DGs is 130A. After the first step at $t = 0.4s$ the load current demand is 100A, and after second step at $t = 0.8s$ it is 150A.

Before $t = 0.8s$, the voltage-controlled DG (battery) only supplied the transient current. After $t = 0.8s$, it also supplies the shortfall of $150 - 130 = 20$(A). This happens automatically, without communication, by virtue of voltage control. Therefore, the actual behaviour of the voltage-controlled DG (battery) can be more accurately described as:

$$i_B = i_L - i_{DG} = \begin{cases} i_L \frac{s\tau}{1+s\tau} & if\ i_{DG}^{max} \geq i_L \\ i_{DG}^{max} \frac{s\tau}{1+s\tau} + (i_L - i_{DG}^{max}) & if\ i_{DG}^{max} < i_L \end{cases} \quad (14)$$

where i_{DG}^{max} is the total current capacity of all current controlled DGs.

In the above examples it was assumed that load behaves as a "current source", i.e. that the load current step change is driving the DC microgrid currents. Such loads are known in power systems as constant current loads (CCL). A more realistic load model is a combination of constant impedance load (CIL) and constant power load (CPL). CPL normally poses a challenge for microgrid stability because it compensates for a voltage reduction by drawing more current, which causes a further voltage reduction, etc [19].

However, the current-driven power sharing mechanism described in this section is immune to the destabilizing effect of CPL. It can be shown that, in the presence of any type of loads, the same fundamental microgrid equations, expressed in terms of i_L and i_{DG}, stand:

$$i_L(t) = i_{DG}(t) + \tau \frac{di_{DG}(t)}{dt} \quad (15)$$

$$v_L(t) = v_{PCC} - (R_B + R_{DG}) i_L(t) + R_{eq} i_{DG}(t) \quad (16)$$

where $R_{eq} = R_B + (1 - \alpha) R_{DG}$.

After substituting $i_L = v_L/R_L$ (for CIL) or $i_L = P_L/v_L$ (for CPL) into (16), expression for i_L in terms of i_{DG} can be obtained, as shown in Table I as $i_L(i_{DG})$. Substituting this expression into (15) allows to solve for $i_{DG}(t)$, and to find $i_B(t) = i_L(t) - i_{DG}(t)$. For all load types, the resulting currents have the forms given by (10) and (11), albeit with different i_L^o and i_L^s values and different values of time constant τ', as detailed in Table I.

TABLE I
PARAMETERS FOR DIFFERENT LOAD TYPES

Parameter	CIL	CPL
$i_L(i_{DG})$	$\dfrac{V_{PCC} + R_{eq} i_{DG}}{R_L + R_{DG} + R_B}$	$\dfrac{V_{PCC} - \dfrac{R_{eq} i_{DG}}{f(P_L)}\left(1 - f(P_L)^a\right)}{2(R_{DG} + R_B)}$
i_L^o	$\dfrac{V_{PCC}}{R_L^o + \alpha R_{DG}}$	$\dfrac{V_{PCC}\left(1 - f(P_L^o)\right)}{2(R_{DG} + R_B) + R_{eq}\left(\dfrac{1}{f(P_L^o)} - 1\right)}$
i_L^s	$\dfrac{V_{PCC}}{R_L^s + \alpha R_{DG}}$	$\dfrac{V_{PCC}\left(1 - f(P_L^s)\right)}{2(R_{DG} + R_B) + R_{eq}\left(\dfrac{1}{f(P_L^s)} - 1\right)}$
τ'	$\tau \dfrac{R_L^s + R_{DG} + R_B}{R_L^s + \alpha R_{DG}}$	$\tau \dfrac{2(R_{DG} + R_B)}{2(R_{DG} + R_B) + R_{eq}\left(\dfrac{1}{f(P_L^o)} - 1\right)}$

[a] where $f(P_L) = \sqrt{1 - 4P_L(R_{DG} + R_B)/V_{PCC}^2}$

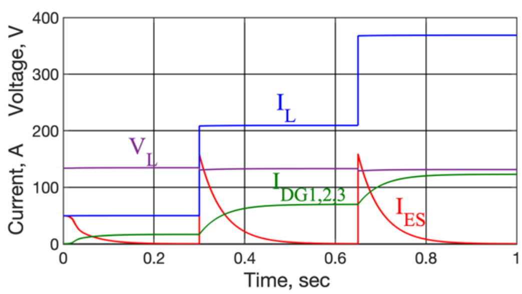

(a) Constant Current Load (CCL)

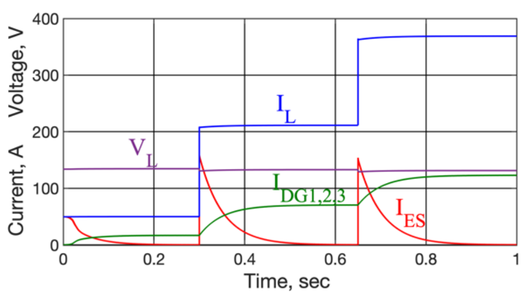

(b) Constant Impedance Load (CIL)

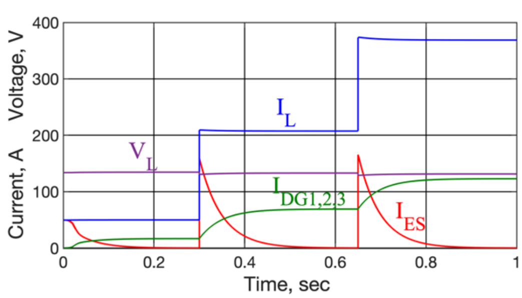

(c) Constant Power Load (CPL)

Fig. 5 Response to load step changes of the example microgrid

Therefore, the current-driven power sharing microgrid exhibits simple and stable first-order dynamics regardless of the load type. This is illustrated in Fig.5, for a DC microgrid with three equally rated current controlled DGs connected to a CCL (see Fig.5(a)), CIL (see Fig.5(b)) and CPL (see Fig.5(c)) loads. Compared to CCL, the differences are very minor and include: a slightly slower dynamics and a small i_L undershoot for CIL, and a slightly faster dynamics and a small i_L overshoot for CPL.

III. AC MICROGRIDS

Where a microgrid is expected to merge with the existing AC infrastructure, AC microgrid option may be given a preference. The current-driven power sharing concept described in the previous section, can be easily adapted to AC microgrids. If a rotating dq-frame is associated with measured AC bus voltage at the coupling point, then the following expressions will describe voltage across the coupling inductor [20]:

$$\begin{cases} v_{Sj}^d = R_j i_{Sj}^d + L_j \dfrac{d i_{Sj}^d}{dt} + \left(v_j - \omega L_j i_{Sj}^q\right) \\ v_{Sj}^q = R_j i_{Sj}^q + L_j \dfrac{d i_{Sj}^q}{dt} + \left(\omega L_j i_{Sj}^d\right) \end{cases} \quad (17)$$

where $v_{Sj}^{d,q}$ is output voltage of the DGj inverter;

v_j is voltage at the coupling point (due to its alignment with d-axis, $v_{Sj}^d = v_j$ and $v_{Sj}^q = 0$);

$i_{Sj}^{d,q}$ is the current supplied by the DGj inverter;

L_j is inductance and R_j is resistance of the coupling inductor;

$\omega = 2\pi f$ is the angular frequency the dq-frame rotation corresponding to the AC microgrid frequency f.

DG converter can be implemented as a current controlled Voltage Source Inverter (VSI). Control diagram for inverter DGj is shown in Fig.6(a) for one axis only (d or q). Such a control block, in AC microgrid, replaces the corresponding current control section in DC microgrid depicted in Fig.3(b).

Current reference $i_{Sj}^*(i_{Sj}^{d*}, i_{Sj}^{q*})$ used by the control is formed from the corresponding measured downstream current $i_j(i_j^d, i_j^q)$ by applying the share D_j. Controller $C(s)$ is a PI regulator with gain 1, and K_j is chosen as per (8). Voltage v_j^*, fed-forward to the VSI reference, corresponds the cross-coupling compensation for the terms appearing in (17) in brackets: $v_j^{d*} = v_j - \omega L_j i_{Sj}^q$ and $v_j^{q*} = \omega L_j i_{Sj}^d$.

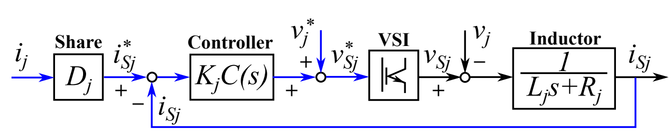

(a) Current controlled VSI used as DG power converter

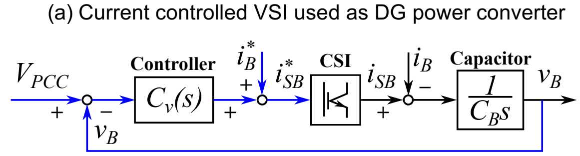

(b) Voltage controlled CSI as BSS power converter

Fig. 6 Implementations of DG and BSS converter control

If the time constant of the PI controller matches the inductor's time constant $\tau = L_j/K_j$, then the closed loop transfer function from the reference i_{Sj}^* to the actual current i_{Sj} is given by $1/(1 + s\,L_j/K_j)$, which is identical to the dynamics of DGj converters described in section II. This leads to the combined DG dynamics as per expressions (12), which is interpreted in the context of AC microgrid as low frequency "envelopes" of the corresponding AC currents.

For the voltage controlled (battery) inverter, a voltage controlled current source inverter (CSI) is an appropriate choice.

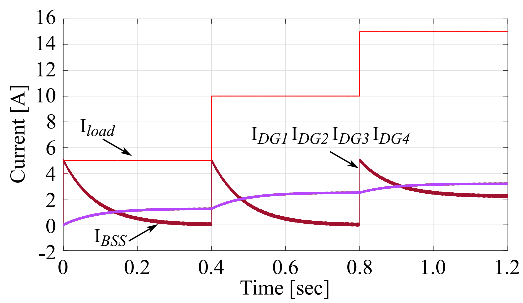

(a) Equal DGs, d-currents, unity power factor

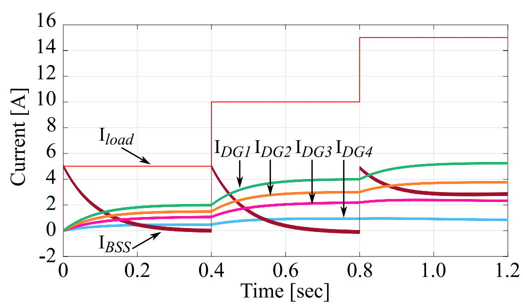

(b) Unequal DGs, d-currents, unity power factor

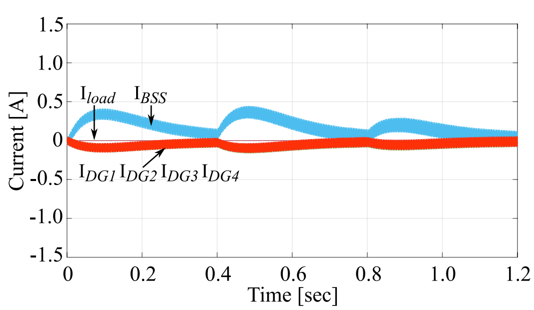

(c) Equal DGs, q-currents, unity power factor

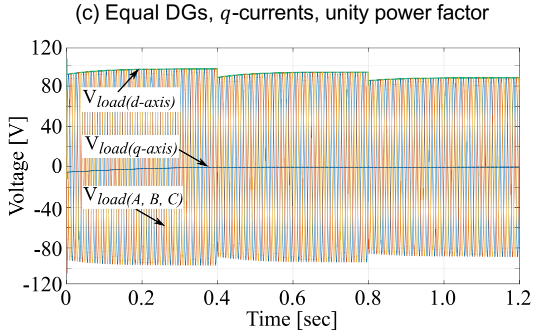

(d) Load voltages, unity power factor

Fig. 7 AC microgrid under current-driven power sharing

It can be implemented directly, as shown in Fig. 6(b), or indirectly (when CSI is implemented as a VSI with a fast current control loop around it).

Simulation results for an AC microgrid under the current-driven power sharing, for inverters with equal and non-equal power ratings, are shown in Fig.7. In both cases, each DG injects its current at unity power factor to the coupling voltage.

IV. POWER LINE COMMUNICATION

Both DC and AC microgrids described in the previous sections did not utilize any form of explicit communication. However, the settings (D_j, K_j) of each individual DG converter depended on the knowledge of its share with respect the total current capacity $\sum_{j=1}^{N} i_{Sj}$, i.e. on the global information.

It is possible that some DG converters are taken out or brought into operation, or that energy available to some of the DG converters changes over time. Under the current-driven power sharing, any deficit in DG power generation is automatically shifted towards the leftmost DG with share $D_N = 1$. If it reaches its full capacity, then the deficit is automatically supplied by battery, as per (14). However, to avoid an unnecessary discharge of the battery, it may be desirable that the DGs remaining in operation communicate changes and adjust their shares in the power generation accordingly.

The standard approach for Master-Slave or Droop control schemes is to use a low bandwidth communication channel between Master and Slaves, or between the Secondary Control and DGs, respectively. Similarly, low bandwidth communication can be added to the current-driven power sharing scheme as well. However, a much more elegant and practical approach is to use the main current stream as the medium for low bandwidth Power Line Communication (PLC).

Power Line Communication (PLC) is a specific form of low bandwidth communication, which utilizes the power infrastructure as the communication medium, and contains all the information within it. The PLC concept has been successfully applied in distribution networks [21] and is currently being adopted in microgrids. The existing applications of PLC include the support of Battery Management Systems [22], remote loads [23] and renewable sources [24].

Under the current-driven power sharing, all DGs are interconnected via a shared unidirectional current stream. To enable PLC in such an environment, each DG should be continuously receiving, removing and reinjecting information. Hence the PLC control needs to be seamlessly merged with the main control loops, as described below.

For the purpose of the PLC implementation, it is logical that the DG inverter takes its current measurement upstream, as shown in Fig.8(a), rather than downstream, as in Fig.3(a). Then the downstream current (i_j) that is needed for the purpose of current control can be obtained by summing the upstream (i_{j+1}) and the DG's own (i_{Sj}) currents as shown in Fig.8(b).

A pre-determined frequency range, free of harmonics, can be dedicated to PLC (e.g., 560Hz to 640Hz). The PLC signal may take a form of a high-frequency pulse, whose duration contains information about the loading condition (in % rated) of the sending DG. Alternatively, the PLC signal may have a variable frequency (within the given range), and the loading condition may be coded in the frequency itself (e.g., 560Hz means zero, 640Hz means 100% of the rated power) [9].

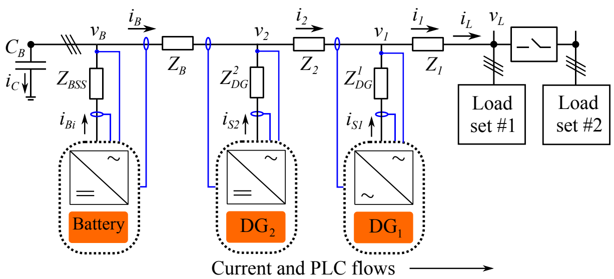

(a) Microgrid measurement configuration when using PLC

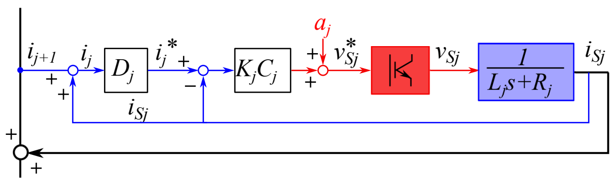

(b) Control of each DG control with the PLC signal injection

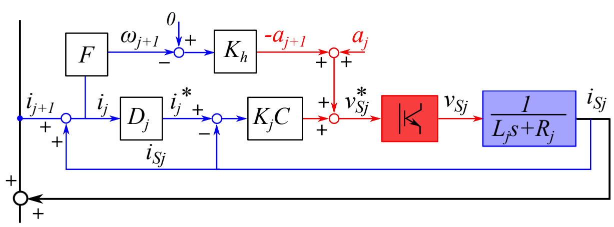

(c) Extended DG control including the PLC compensation

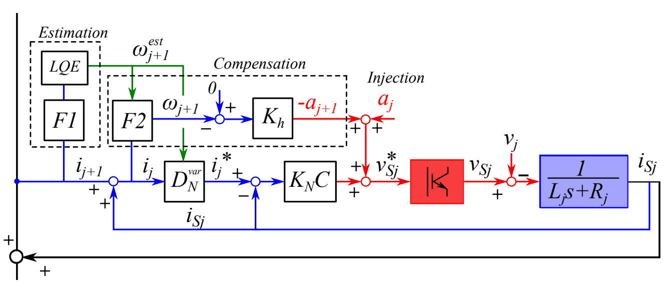

(d) A further extension showing the PLC frequency estimation

Fig. 8 Merging PLC with the microgrid current control

The core idea is that each DG converter receives a PLC signal, mixed in the current stream, from its upstream neighbour. After receiving the PLC information, each DG converter removes the previous PLC signal and reinjects its own PLC signal into the stream. This PLC signal is then received by the next DG inverter downstream, etc.

Fig.8(b) shows the main current control, with the PLC injection point denoted as a_j. It follows that

$$v_{Sj}^{*}=v_{Sj,cc}^{*}+a_j=v_{Sj,cc}^{*}+A\sin(\omega_{PLC}t) \qquad (18)$$

where $v_{Sj,cc}^{*}$ is the reference voltage driving the main current control (without PLC);

A and ω_{PLC} are the magnitude and the frequency of the PLC signal, respectively.

The PLC signal a_{j+1} received from the upstream DG, needs to be removed. A feedback compensation loop with gain K_h and high-pass filter F, as shown in Fig.8(c), drives to zero the presence of a_{j+1} signal in the downstream current by implicitly adding $-a_{j+1}$ at the injection point.

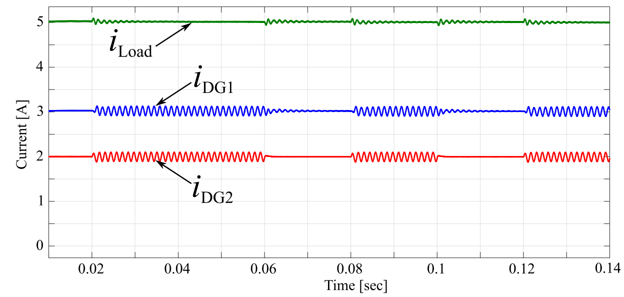

(a) PLC suppression: DC currents

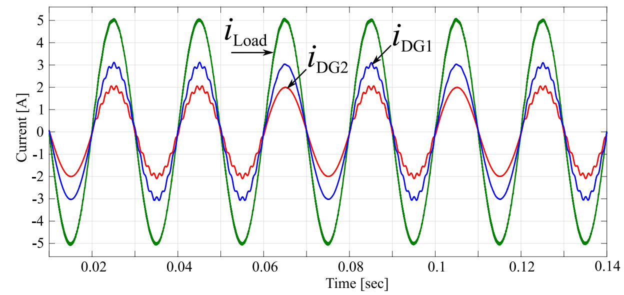

(b) PLC suppression: AC currents

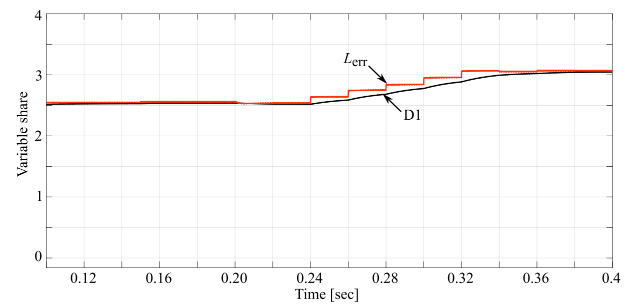

(c) Adjustment of DG share by a slow integrator

Fig. 9 PLC signal reception and suppression

For PLC at variable frequency, estimation of the PLC frequency is further necessary. This can be achieved, for example, by using a Linear Quadratic Estimator (LQE) as shown in Fig.8(d).

Using the described techniques, the upstream PLC signal a_{j+1} is received and removed from the stream, and the new PLC signal a_j is injected in downstream. The last DG (closest to the load) receives, removes and does not inject any further PLC signal. This is illustrated in Fig.9, for the cases of DC microgrid (see Fig.9(a)) and AC microgrid (see Fig.9(b)).

The information contained in the PLC may be used by each DG to equalize its % loading with its neighbouring DG. This can be achieved by adding a slow integral control that adjusts the share D_j based on the error between the % loading of the DGj and that of its upstream neighbour DG(j+1). This is illustrated in Fig.9(c).

The fact that deficit in power generation is shifted by the main current control upstream (towards the battery side) but the %

loading is communicated via PLC in the downstream direction (from the battery to the load side), leads to equalization of the % loading of all DGs in steady state. This is illustrated by a scenario shown in Fig.10.

The initially equal power sharing between four DGs was perturbed at $t = 2$s by DG3 losing half of its power. The deficit was transferred by the current sharing mechanism to DG4 (since its share in the downstream current was $D_4 = 1$). However, this caused the rise of the DG4 % loading, which it communicated by increasing the PLC frequency $\omega_{q,4}$.

The next DG downstream was DG3 who was "at fault" and could not increase its generation any further. It simply allowed the PLC signal to pass downstream. The next was DG2 who, in response to the PLC signal, started increasing its loading and communicated that to DG1. As a result, DG1, DG2 and DG4 arrived at new and equal shares around $t = 4$s.

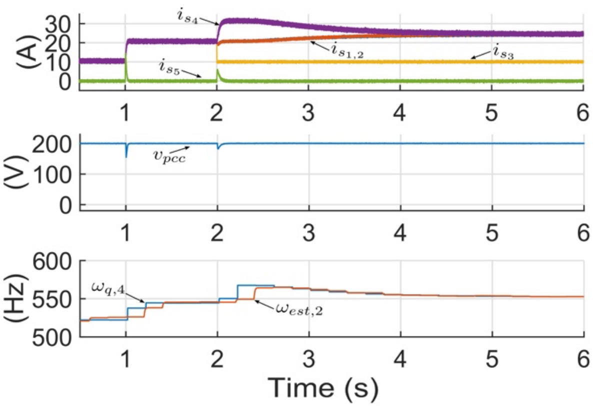

Fig. 10 DG current adjustment by using PLC (simulation)

V. CONCLUSION

This paper has discussed the growing utilization of renewable energy in mining industry, via its integration into microgrids. It has reviewed the microgrid control principles and popular schemes. The paper has provided a detailed description of a specific, current-driven, microgrid control strategy that achieves power sharing of current controlled distributed generators without explicit communication, by utilizing specially organized current measurement in the shared current stream and appropriate selection of the control gains.

The paper has demonstrated simplicity, stability, compatibility with all load types, and applicability of the current-driven power sharing to DC and AC microgrids. While, under this approach, the need for the Secondary Control Similar is eliminated, there may be a need for occasional share readjustments following changes in a microgrid structure. The paper has shown that such adjustments can be achieved by integrating Power Line Communication into the microgrid current control.

The microgrid control principles discussed in the paper offer benefits to various applications in mining industry and beyond.

VI. REFERENCES

[1] L. Delevingne, W. Glazener, L. Gregoir, and K. Henderson, "Climate risk and decarbonization: What every mining CEO needs to know," *McKinsey Sustainability*, pp. 1–1, January 2020.

[2] L. Liu, H. Ji, X. Lu, T. Wang, S. Phi, F. Pei, and D. Quan, "Mitigation of greenhouse gases released from mining activities: A review," *International Journal of Minerals, Metallurgy and Materials*, no. 28, pp. 513–521, 2021.

[3] C. Karacan, F. Ruiz, M. Cote, and S. Phipps, "Coal mine methane: A review of capture and utilization practices with benefits to mining safety and to greenhouse gas reduction," *International Journal of Coal Geology*, vol. 86, no. 2, pp. 121–156, 2011.

[4] International Mining Team Publishing Ltd, "Hydrogen trucks: News Archive." [Online]. Available at https://im-mining.com/, 2022.

[5] "IEEE 2030-2011 - Guide for Smart Grid Interoperability of Energy Technology and Information Technology Operation with the Electric Power System (EPS), End-Use Applications, and Loads," 2011.

[6] S. K. Sahoo, A. K. Sinha, and N. K. Kishore, "Control techniques in AC, DC, and hybrid AC-DC microgrid: A review," *IEEE Journal of Emerging and Selected Topics in Power Electronics*, vol. 6, no. 2, pp. 738 – 759, 2018.

[7] M. S. Golsorkhi, Q. Shafiee, D. D.-C. Lu, and J. M. Guerrero, "Distributed control of low-voltage resistive ac microgrids," *IEEE Transactions on Energy Conversion*, vol. 34, no. 2, pp. 573 – 584, 2019.

[8] H. Han, X. Hou, J. Yang, J. Wu, M. Su, and J. M. Guerrero, "Review of power sharing control strategies for islanding operation of ac microgrids," *IEEE Transactions on Smart Grid*, vol. 7, no. 1, pp. 200 – 215, 2017.

[9] D. Miller, G. Mirzaeva, C. D. Townsend, and G. C. Goodwin, "The use of power line communication in standalone microgrids," *IEEE Transactions on Industry Applications*, vol. 57, no. 3, pp. 3029–3037, 2021.

[10] A. Nazib, D. Holmes, and B. McGrath, "Autonomous current sharing control with integrated virtual impedance and self synchronisation for unbalanced islanded microgrids," in *2020 IEEE Energy Conversion Congress and Exposition (ECCE)*, pp. 3872–3879, 2020.

[11] G. Mirzaeva, C. D. Townsend, D. Semenov, and G. C. Goodwin, "Decentralised control of parallel inverters in an ac microgrid using downstream current as an implicit communication method," in *2017 IEEE Southern Power Electronics Conference (SPEC)*, 2017.

[12] G. Mirzaeva, D. Miller, G. Goodwin, and P. Wheeler, "A stable and robust dc power system for more electric aircraft," in *Proc. of 2021 IEEE ECCE*, pp. 5196–5201, 2021.

[13] M. Choobineh, D. Silva-Ortiz, and S. Mohagheghi, "An automation scheme for emergency operation of a multi-microgrid industrial park," *IEEE Transactions on Industry Applications*, vol. 54, no. 6, pp. 6450– 6459, 2018.

[14] J. S. Gomez, J. Llanos, E. Espina, C. Burgos-Mellado, and J. Rodriguez, "Cooperative power conditioners for microgrids in mining," in *2021 23rd European Conference on Power Electronics and Applications (EPE'21 ECCE Europe)*, pp. P.1–P.10, 2021.

[15] J. S. Gomez, J. Rodriguez, C. Garcia, L. Tarisciotti, F. Flores-Bahamonde, J. Pereda, F. Nunez, A. Z. Cipriano, and J. C. Salas, "An overview of microgrids challenges in the mining industry," *IEEE Access*, vol. 8, pp. 191378–191393, 2020.

[16] C. Yuan, M. A. Haj-ahmed, and M. S. Illindala, “Protection strategies for medium-voltage direct-current microgrid at a remote area mine site,” *IEEE Transactions on Industry Applications*, vol. 51, no. 4, pp. 2846– 2853, 2015.

[17] M. G. Jahromi, G. Mirzaeva, S. D. Mitchell, and D. Gay, “Dc power vs ac power for mobile mining equipment,” in *2014 IEEE Industry Application Society Annual Meeting*, pp. 1–8, 2014.

[18] E. Hossain, R. Perez, A. Nasiri, and S. Padmanaban, “A comprehensive review on constant power loads compensation techniques,” *IEEE Access*, vol. 6, pp. 33285 – 33305, 2018.

[19] J. Chen and J. Chen, “Stability analysis and parameters optimization of islanded microgrid with ideal and dynamic constant power loads,” *IEEE Transactions on Industrial Electronics*, vol. 65, no. 4, pp. 3263 – 3274, 2018.

[20] R. S. Pena, R. J. Cardenas, G. M. Asher, and J. C. Clare, “Vector controlled induction machines for stand-alone wind energy applications,” in *IAS 2000 - 35th Annual Meeting the IEEE Industry Applications Society*, vol. 3, pp. 1409 – 1415, 2000.

[21] G. Lopez, J. Matanza, D. De La Vega, M. Castro, A. Arrinda, J. I. Moreno, and A. Sendin, “The role of power line communications in the smart grid revisited: Applications, challenges, and research initiatives,” *IEEE Access*, vol. 7, 2019.

[22] J. Jousse, Ginot, C. Batard, and E. Lemaire, “Power line communication management of battery energy storage in a small-scale autonomous photovoltaic system,” *IEEE Transactions on Smart Grid*, vol. 8, no. 5, 2017.

[23] G. I. C. Lobato, S. M. Silva, F. V. Amaral, and B. J. C. Filho, “Powerline communication (PLC) through power converter’s DC bus: Applicability assessment,” in *2015 IEEE 13th Brazilian Power Electronics Conference and 1st Southern Power Electronics Conference (COBEP/SPEC)*, 2015.

[24] [24] S. C. Pereira, A. L. L. F. Murari, C. E. Capovilla, J. A. T. Altuna, R. V. Jacomini, A. Belati E, S. Filho A J, and I. R. S. Casella, “Enabling smart grid concept in wind farms by means of power line communication technology,” in *2018 13th IEEE International Conference on Industry Applications (INDUSCON)*, 2018.

VII. VITAE

Galina Mirzaeva received BEng degree in electronic engineering in 1990 and PhD in electrical engineering in 1997 from the South Urals State University, Russia.

From 2004 to 2010, she worked at CRC-Mining, Australia. Since 2010, she has been with the School of Engineering at the University of Newcastle, Australia, first as Senior Lecturer and from 2017 - as Associate Professor.

Her research interests include power electronics, electric drives, and renewable energy integration and electric transportation. Dr Mirzaeva currently serves as Chair of the IEEE IAS Mining Industry Committee.

Dmitry Miller received BEng degree in power engineering from Ural Federal University, Ekaterinburg, Russia, in 2014. In 2020 he received MS degree in electrical engineering at Harbin Institute of Technology, Harbin, China. In 2021 he received PhD degree in electrical engineering from The University of Newcastle, Australia.

His research interests include power electronics, electric drives, microgrids and electric transportation. Dr Miller currently works as Engineer at Ampcontrol CSM (Australia).